Rapid Prediction of Effect of Localized Spallation of Thermal Barrier Coatings on Blade Cooling Efficiency Based on an MLP Neural Network

ZHANG Yeling[1], *WANG Feilong*[1*], *WANG Yuqun*[2], *WANG Yubin*[1], *MAO Junkui*[1]

1. College of Energy and Power Engineering, Nanjing University of Aeronautics and Astronautics, Nanjing 210016, P. R. China; 2. AECC Sichuan Gas Turbine Establishment, Chengdu 610500, P. R. China

(Received 25 April 2025; revised 16 August 2025; accepted 12 October 2025)

Abstract: The study of the spallation of thermal barrier coatings on turbine blades and its influence is of great significance for gas turbine safety operation. However, numerical simulation related to thermal barrier coatings is difficult and time-costly, which makes it hard to meet engineering demands. Therefore, this work establishes a rapid prediction model for the surface temperature and cooling efficiency of turbine blades with localized spallation of thermal barrier coatings based on a thin-wall thermal resistance model. Firstly, the influence of localized spallation of thermal barrier coatings on the cooling efficiency of typical turbine blades is numerically investigated. Then, based on the simulation data set and multi-layer perception (MLP) neural network, an intelligent prediction model for the temperature and cooling efficiency distribution of localized spallation of coatings is constructed, which can rapidly predict the surface temperature and cooling efficiency of the blade under the situation of spallation of coating at any position on the blade surface. The results show that, under a certain spallation area, the shape of localized coating spallation has little influence on the cooling efficiency, while the increase of spallation thickness will cause a linear increase in the average temperature of the blade surface. The prediction error of the proposed rapid prediction model for the average surface temperature and cooling efficiency of blades is within 2%, and the prediction error of the temperature and cooling efficiency at the spallation position is within 6% for 80% of the samples, with an overall average error within 10%. It is concluded from the rapid prediction model that when the depth of coating spallation increases, the closer the spallation position is to the leading edge of the blade, the greater the difference in cooling efficiency is, and the degree of influence of coating spallation on the cooling efficiency also increases.

Key words: thermal barrier coating (TBC); cooling performance; rapid prediction; multi-layer perception (MLP) neural network

CLC number: V232.4 **Document code:** A **Article ID:** 1005-1120(2025)06-0813-17

0 Introduction

The thermal barrier coating (TBC) technology is now widely used in the aerospace field as a thermal protective layer for various component structures[1-2]. With the continuous improvement of the efficiency of gas turbines, the inlet temperature of the turbine keeps rising and gradually exceeds the temperature limit of traditional nickel-based superalloy blades[3]. Although the excellent thermal insulation properties of TBCs provide some protection against blade ablation, the coatings are subjected to high-temperature oxidation, particle impact erosion, and the harsh working conditions caused by calcium magnesium aluminum silicate (CMAS) molten salt erosion. These factors have directly compromised the thermal insulation performance of coatings, lead-

*Corresponding author, E-mail address: wangfl@nuaa.edu.cn.

How to cite this article: ZHANG Yeling, WANG Feilong, WANG Yuqun, et al. Rapid prediction of effect of localized spallation of thermal barrier coatings on blade cooling efficiency based on an MLP neural network[J]. Transactions of Nanjing University of Aeronautics and Astronautics, 2025, 42(6): 813-829.

http://dx.doi.org/10.16356/j.1005-1120.2025.06.008

ing to a higher probability of local failure and spallation[4]. This phenomenon will cause changes in the comprehensive cooling efficiency of turbine blades, thereby affecting the working intensity and operational stability of the engine; therefore the study of the spallation of thermal barrier coating on the surface of turbine blades is of great significance for the safe operation of gas turbines.

With the development of modern technology, numerical methods have gradually been developed and utilized in the related research of TBC. The existing numerical simulation models of turbine blades with thermal barrier coatings have established a foundational framework[5-6]. The simplified models can better predict the stress field and temperature conditions of turbine blades. However, if the actual temperature distribution of turbine blades and their complex geometric structures are considered, the fluid-solid coupling and conjugate thermal transfer of blade models still need to be developed urgently. In recent years, many scholars have conducted relevant research on the stress distribution[7-8] and crack propagation characteristics[9-11] of the TBC system during the thermal cycling process, and obtained the physical property characteristics of the thermal barrier coating. However, there are still deficiencies in the research on the influence of thermal barrier coating spallation on the cooling efficiency of hot-end components. Additionally, numerical simulation methods for thermal barrier coatings still face limitations, such as fine mesh division, high iterative calculation costs, and long computation times, which make them challenging to apply to engineering demands. To deal with these challenges, the application of artificial intelligence such as machine-learning algorithms and regression analysis predictive modeling techniques has become a trend in simulation research[12]. By training the proxy model to learn the volvement rule of fluid field and directly predicting the simulation results, the computing time can be significantly reduced. Moreover, the proxy model is capable of learning multi-physics and multi-scale information, enabling rapid prediction of performance across different parameter combinations. In the related research on predicting the failure spallation of TBC, Yang et al.[13] proposed a method of processing acoustic emission signals based on the wavelet packet transform and neural networks. The four typical failure modes of TBC coatings can be discriminated through this method, thereby monitoring the failure mechanism of TBC in real time and evaluating its service reliability. Liu et al.[14] comprehensively considered the failure mechanisms such as oxidation, creep, and thermal mismatch during the failure process of thermal barrier coatings, as well as various factors such as the combined effect of gas and coolants at both the micro and macro scales, and established a multi-scale life prediction model integrating artificial neural networks for the failure prediction of turbine blade coatings. This model has a good prediction effect on the failure area of thermal barrier coating on the surface of turbine blades.

At present, most of the research related to TBC focuses on coating failure mechanisms and life prediction, etc., while relatively few studies examine the decline in component cooling efficiency after the coating spallation. Meanwhile, although some scholars have established multi-scale life prediction models integrating artificial neural networks for the failure prediction of turbine blade coatings, these models still have certain limitations in terms of prediction accuracy, application scope, and adaptability to complex working conditions. Therefore, based on machine learning methods, this work conducts a rapid prediction study on the influence of localized spallation of thermal barrier coatings on the cooling efficiency of blades, aiming to accurately and rapidly predict the influence of coating spallation on the heat transfer of turbine blades, which has certain guiding significance for the life prediction of turbine blades.

1 Physical Models and Numerical Methods

1.1 Physical model

In this work, the C3X blade without radial distortion is selected as the research object. The blade height is 76.2 mm, the cascade pitch is 117.73 mm,

the axial chord length is 78.16 mm, the blade chord length is 144.93 mm, and the blade material is 310 stainless steel of ASTM standard, which has a relatively low thermal conductivity. The cross-sectional schematic diagram of the blade and its cascade channel is shown in Fig.1(a), and the specific geometric and physical parameters of the blade model are presented in Table 1. It should be noted that the blade thermal conductivity is temperature-dependent and is calculated as $\lambda=9.910\ 5+0.011\ 5T$, where T is the local temperature of the blade material (solid domain) at each location. The surface of the blade is uniformly coated with a thermal barrier coating with a thickness of 0.35 mm. Its equivalent physical parameters include the density of 5 650 kg/m^3, thermal conductivity of 1.05 W/(m·K), and specific heat capacity of 483 J/(kg·K)[15]. Fig.1(b) presents the physical model of the C3X blade and the setting of boundary conditions. This work selects the corresponding working conditions of the No.4521 test in Ref.[16] for numerical research. The specific parameter settings of the boundary conditions are shown in Table 2. The blade is equipped with ten circular radial cooling channels. The cross-sectional geometric dimensions of each channel and the cold air inlet conditions are shown in Table 3.

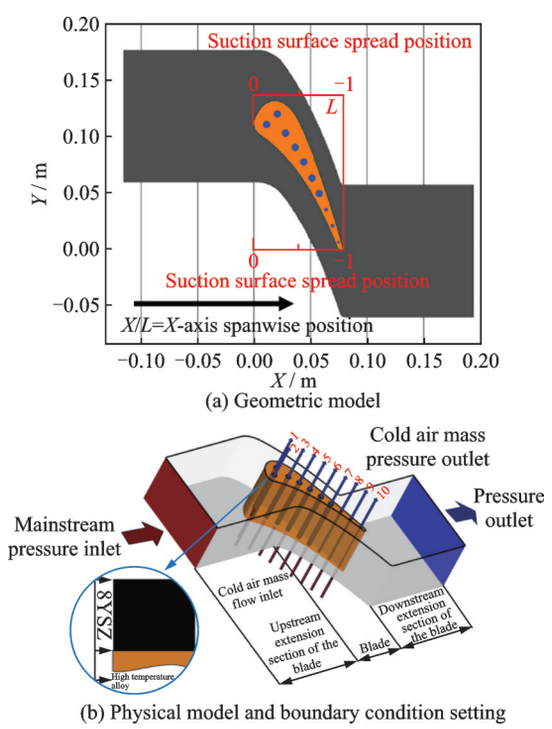

Fig.1 C3X blade model and boundary condition setting

Table 1 Blade geometric and physical parameters

Geometric parameter	Numerical value
Leaf grid pitch τ/ mm	117.73
Blade height H/ mm	76.2
Axial chord length C_{ax} / mm	78.16
Blade chord length C_x / mm	144.93
Density ρ/ (kg•m^{-3})	8 030
Specific heat c/ (J•kg^{-1}•K^{-1})	502.48
Thermal conductivity λ/(W•m^{-1}•K^{-1})	$9.910\ 5+0.011\ 5T$

Table 2 Boundary conditions for Test No.4521 in Ref.[16]

Test condition	Parameter	Value
Heat flow inlet boundary condition	Total inlet pressure/Pa	413 286
	Total inlet temperature/K	818
	Inlet turbulence intensity/%	8.3
	Import viscosity ratio	30
	Import Mach number	0.17
	Inlet Reynolds number	6.4×10^6
Heat flow outlet boundary condition	Outlet static pressure/Pa	254 172
	Export Mach number	0.89
	Outlet Reynolds number	2.44×10^6

Table 3 Blade internal cooling channel inlet conditions

Channel number	Diameter/mm	Flow rate/ (kg•s^{-1})	T_{in}/K
1	6.3	0.022 2	342
2	6.3	0.022 1	344
3	6.3	0.021 8	335
4	6.3	0.022 8	336
5	6.3	0.022 5	330
6	6.3	0.022 5	355
7	6.3	0.021 6	336
8	3.1	0.007 44	350
9	3.1	0.004 77	377
10	1.98	0.002 56	387

1.2 Numerical calculation method

1.2.1 Flow control equation

The flow of high-temperature gas and cold air is a three-dimensional steady-state compressible flow. The flow heat transfer among gas, blades and cold air, as well as the heat transfer between blades and coatings, and the heat transfer within blades all conform to the conservation of mass, momentum and energy. In the usual sense, the control equation is the partial differential expression of the above three conservation laws. The three conservation equations can be expressed as

Continuity equation

$$\nabla\cdot(\rho_{\mathrm{f}}\boldsymbol{V})=0 \tag{1}$$

where ρ_{f} is the fluid density and $\boldsymbol{V}$ the fluid velocity vector. The term $\nabla\cdot(\rho_{\mathrm{f}}\boldsymbol{V})$ represents the divergence of the mass flux.

Momentum equation

$$\nabla\cdot(\rho_{\mathrm{f}}\boldsymbol{V}\boldsymbol{V})=-\nabla p+\nabla\cdot\boldsymbol{\tau}+\rho_{\mathrm{f}}f \tag{2}$$

where $\boldsymbol{V}\boldsymbol{V}$ denotes the dyadic (tensor) product of the velocity vector and it is a second-order tensor; the term $\nabla\cdot(\rho_{\mathrm{f}}\boldsymbol{V}\boldsymbol{V})$ the divergence of the convective (advective) momentum flux; $-\nabla p$ the pressure-gradient force (directed toward decreasing pressure); $\boldsymbol{\tau}$ the viscous stress tensor and $\nabla\cdot\boldsymbol{\tau}$ the divergence of the viscous stress; and $\rho_{\mathrm{f}}f$ the body-force term per unit volume.

Energy conservation equation

$$\nabla\cdot(\rho_{\mathrm{f}}\boldsymbol{V}h)=\nabla\cdot(\lambda\nabla T)+\boldsymbol{V}\cdot\nabla p+\boldsymbol{\tau}:\nabla\boldsymbol{V} \tag{3}$$

where $\nabla\cdot(\rho_{\mathrm{f}}\boldsymbol{V}h)$ is the divergence of the convective enthalpy flux with h being the specific enthalpy; the term $\nabla\cdot(\lambda\nabla T)$ heat conduction (diffusion) with λ being the thermal conductivity and T the fluid temperature; $\boldsymbol{V}\cdot\nabla p$ the pressure-work term; $\boldsymbol{\tau}:\nabla\boldsymbol{V}$ the viscous dissipation term, accounting for the conversion of mechanical energy into internal energy due to viscous effects; the symbol ":" indicates the double contraction of tensors; $\nabla\boldsymbol{V}$ the velocity-gradient tensor, and $\boldsymbol{\tau}$ the viscous stress tensor with its component expressed as

$$\tau_{ij}=2\mu\left(s_{ij}-\frac{1}{3}\frac{\partial\nu_k}{\partial x_k}\delta_{ij}\right) \tag{4}$$

where μ is dynamic viscosity; s_{ij} the strain-rate tensor component; ν_k the kth component of the velocity vector $\boldsymbol{V}$; and $\dfrac{\partial\nu_k}{\partial x_k}$ the velocity divergence, i.e., $\nabla\cdot\boldsymbol{V}$.

For the coupled heat exchange problem, the following conditions are met at the fluid-structure interface

$$T_{\mathrm{s}}=T_{\mathrm{f}} \tag{5}$$

$$k\left.\frac{\partial T}{\partial n}\right|_{n}=\lambda\left.\frac{\partial T}{\partial n}\right|_{\mathrm{f}} \tag{6}$$

where T_{s} and T_{f} represent the wall temperatures of solid and fluid, respectively; n represents the normal direction. That is, temperature continuity and heat flux conservation are satisfied at the fluid-solid interface.

1.2.2 Thin-wall thermal resistance model

In thermal barrier coating simulation modeling, the direct modeling method is typically employed, where the thermal barrier coating mesh is generated on the substrate surface based on the coating thickness. However, due to the extremely thin thickness of the thermal barrier coating and the existence of localized spallation phenomena, it is difficult to model and mesh division, and it is hard to guarantee the mesh quality, thereby affecting the simulation accuracy. Therefore, the thermal barrier coating modeling method based on the thin-wall thermal resistance model[17] is suitable for dealing with the localized spallation of the coating. The schematic diagram of the thin-wall thermal resistance method is shown in Fig.2. Its principle is to equivalently simulate the heat insulation effect of the thermal barrier coating by setting different surface layer thermal resistances on the outer surface of the substrate, as shown in

$$R_\lambda=\frac{\Delta x}{\lambda} \tag{7}$$

where R_λ is the thermal resistance of heat conduction of the coating, Δx the thickness of the thermal barrier coating, and λ the thermal conductivity of the wall surface.

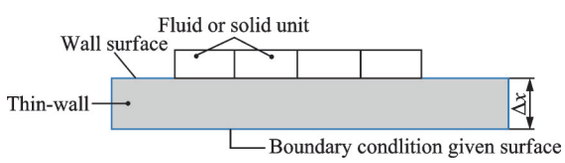

Fig.2 Thin-wall thermal resistance model

In the solution process, the thermal resistance and heat flux of the coating are calculated by solving the one-dimensional steady-state heat conduction equation. Since this model does not alter the geometric structure or size of the substrate, it significantly simplifies modeling and meshing. This approach allows for a quicker assessment of the influence of coating thermal resistance and localized spallation on blade cooling efficiency under varying coating thicknesses and spallation conditions.

Overall, since this study focuses on the steady-state coating spallation issue and mainly concentrates on the macroscopic heat transfer of the coat-

ing, for isotropic thermal barrier coating materials, the heat transfer process is uniform and approximately linearly distributed. Therefore, the numerical differences between the two methods will not have a significant impact on the prediction results.

1.3 Numerical verification

To eliminate the influence of grid division on the results, the grid independence verification is carried out first before conducting numerical calculations. The calculation model is meshed by using Ansys Mesh, and the meshes at the flux-solid interface are encrypted. Meanwhile, in order to reduce the amount of calculation and improve the calculation efficiency, the mesh is appropriately sparsely processed in the area far from the fluid-solid interface and the inlet and outlet sections of the model.

To ensure the independence of grids, seven groups of hexahedral grids with different sparsity levels are divided for numerical calculations. When the number of grids is further increased or decreased, if the average temperature of the blade surface remains basically unchanged, the grid is considered to meet independence requirements. As shown in Fig.3, with the gradual increase of grid quantity, the average temperature of the blade surface gradually decreases. When the number of grids is around 5 million, the average temperature of the blade surface remains basically unchanged. Therefore, this grid is selected for the subsequent numerical research work.

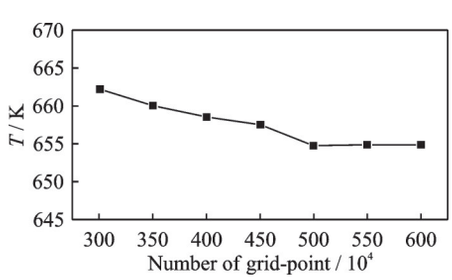

Fig.3 Effect of mesh amount on average blade surface temperature

To further verify the accuracy of the numerical model and select an appropriate turbulence model, this work selects the main and secondary flow conditions No.4521-157 in NASA literature[18], and compares the calculation results with experimental data in the literature. Three turbulence models, namely Standard k-ε, RNG k-ε and SST k-ω, are respectively adopted for numerical calculation, and the pressure ratio and temperature ratio on the mid-span line of the blade are compared with experimental values. Fig.4 shows the pressure ratio distribution along the mid-span of the blade. The vertical coordinate in the figure represents the ratio of the pressure along the mid-span of the blade to the static pressure at the inlet of the cascade channel. As shown in Fig.4, the pressure ratios calculated by the three turbulence models are nearly identical. Due to the gas impact on the leading edge of the blade, the pressure gradient is highest there. The pressure ratio decreases slowly at the pressure surface first. When x is around 0.5, it begins to decrease rapidly. The pressure on the suction surface rises rapidly when x is from -0.4 to 0, while the pressure change near the trailing edge of the suction surface is relatively gentle.

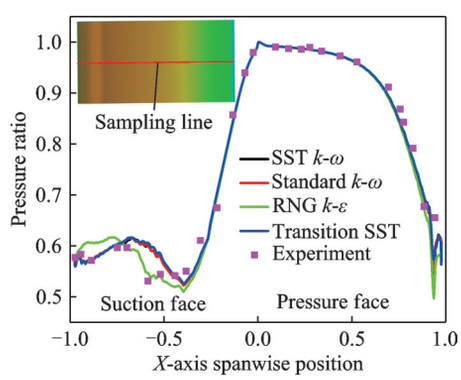

Fig.4 Pressure distribution in the middle sampling line of blade height

Fig.5 presents the comparison between the interline temperature ratios of blades calculated by three turbulence models and experimental values. Among them, the vertical coordinate is the ratio of the blade surface temperature on the mid-span line to the reference temperature (811 K). Due to the gas scouring and the difference in cooling capacity of the cooling channel, the temperatures at the leading edge and trailing edge of the blade are relatively high. It can be seen from Fig.5 that the SST k-ω turbulence model is superior to the other two turbulence models in predicting the surface temperature of blades.

Whether on the pressure surface or the suction surface, the temperature distribution prediction of the SST k-ω model is closer to experimental values than the other two models. Therefore, in the subsequent research of this section, the SST k-ω turbulence model is selected for further analysis.

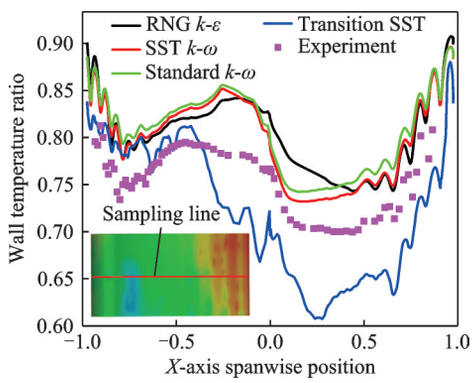

Fig.5 Cross-line temperature distribution on blade surface

2 Influence of Localized Spallation of Thermal Barrier Coating on the Cooling Efficiency

2.1 Modeling methods and effect comparison of thermal barrier coatings

To verify the calculation accuracy of the thin-wall thermal resistance model, a comparison is made with the blade coating directly modeled. The differences between the two methods in terms of heat insulation effect, temperature distribution at localized spallation points, and temperature distribution along the blade surface are analyzed.

Without coating spallation, the surface temperature distribution of the blade at a cut-off line 60 mm away from the blade tip is obtained, as shown in Fig.6. To better illustrate the trend of temperature distribution along the flow path and highlight the temperature difference between the coating surface and its inner layers, the dimensionless parameter $T/811$ is adopted as the vertical coordinate, where 811 K represents the mainstream temperature. It can be seen from the figure that the temperature distribution of the inner and outer surfaces of the coating by the two methods is basically the same. When the coating thickness is 0.35 mm, the average heat insulation temperature of the direct modeling method is 46.53 K, and that of the thin-wall thermal resistance model coating is 44.85 K, with a temperature difference of 1.68 K. Compared with the average heat insulation temperature of the direct modeling method, the error is 3.61%. The maximum insulation temperature point of the coating in the direct modeling method appears at the position where the relative chord length X/L=0.73 and the relative blade height Z/H=0.77. At this point, the temperature difference between the inner and outer surfaces of the coating is 68.12 K. The maximum insulation temperature point of the coating in the thin-wall thermal resistance model appears at the relative chord length X/L=0.80. At the position where the relative blade height Z/H=0.77, the temperature difference between the inner and outer surfaces of the coating at this point is 64.86 K, and the temperature difference from the insulation temperature of the direct modeling method is 3.26 K, with an error of 4.79%. The results show that the coating thickness has a certain impact on the heat insulation effect when using the direct modeling method. However,

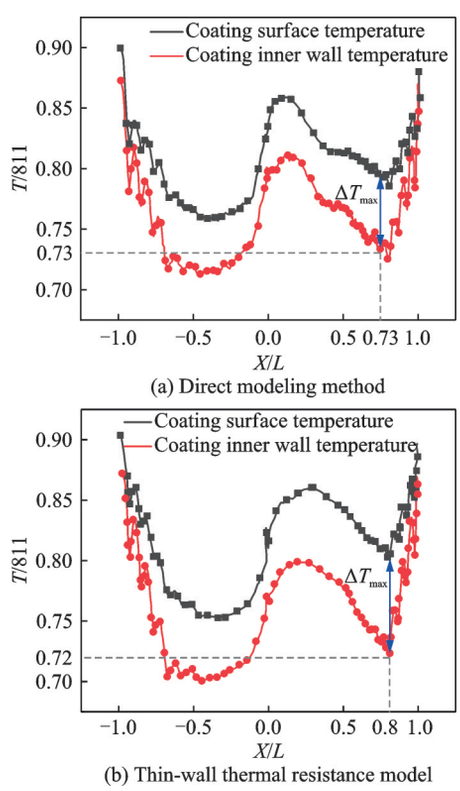

Fig.6 Temperature distribution curves of the inner and outer surfaces of the coating without spallation

by comparing the average and maximum heat insulation temperatures of the entire blade, it is evident that the deviation between the two methods can be controlled within 5%.

The service environment of turbine blades is complex. The thermal barrier coating on the blade surfaces is exposed to a harsh working environment, making localized spallation of the coating inevitable. To investigate the influence of thermal barrier coating spallation on blade cooling efficiency, five critical areas on the blade surface are selected to simulate localized coating spallation. They are respectively one at the leading edge, two at the pressure surface and two at the suction surface, as shown in Fig.7. The shape of the coating spallation is simplified to either circular or rectangular, numbered from 1 to 5. Localized spallation occurs near the middle span line. To investigate the influence of the spallation position on blade cooling efficiency, the localized spallation location is varied along the Z-axis. Positions 1′—5′ represent spallation near the cold air inlet, while positions 1"—5" correspond to spallation near the cold air outlet. The coating of the same area and depth is peeled off at the same position on the blade surface. The blade surface cross-section at a distance of 60 mm from the blade tip is selected. The surface temperature distributions of the two modeling methods on this cross-section are shown in Fig.8. It can be seen that at the trailing edge and the middle part of the suction surface, the surface temperature of the thin-wall thermal resistance model blade is slightly higher than that of the direct modeling method. On the pressure surface and the leading edge section, the average temperature of the blade surface in the direct modeling method is slightly higher than that in the thin-wall thermal resistance model. The average temperature difference and maximum temperature difference on the blade surface of the two methods account for 1.5% and 5.05% of the average temperature on the blade surface respectively, among which the maximum temperature difference is located at $X/L=0.98$. After the same localized spallation occurred in the coatings of the two methods, the insulation temperature

Fig.7 Schematic diagrams of the localized spallation position of the coating

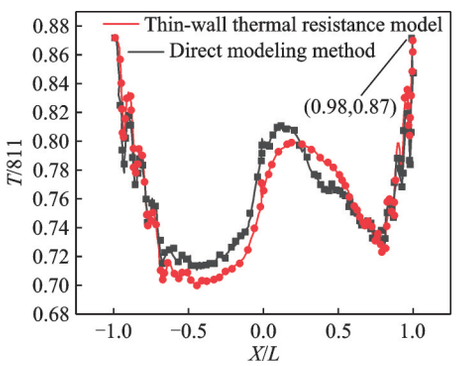

Fig.8 Blade surface temperature distribution curves of two models

of the direct modeling method is 45.13 K, and that of the thin-wall thermal resistance model is 42.32 K, with a temperature difference of 2.81 K, accounting for 6.2%. Within this range, the simulation results of the thin-wall thermal resistance model are comparable to those of the direct modeling method. Furthermore, the thin-wall thermal resistance model does not alter the matrix model structure or geometric dimensions. Therefore, it can significantly reduce the time required for modeling and meshing, effectively simplify the modeling process, address the meshing challenges for thin coatings in direct modeling, and enhance the overall efficiency of coating (localized spallation) modeling and simulation. This is of great significance for rapid and accurate prediction of the impact on heat transfer following localized spallation of thermal barrier coating on turbine blades in actual service environments. In this work, the coating modeling methods in the numerical study of thermal barrier coatings are all based on the thin-wall thermal resistance model.

2.2 Influence of localized spallation of thermal barrier coatings on comprehensive cooling efficiency of blades

Based on the localized spallation positions of

the coating defined in Fig.7, the influence of factors such as the shape, size and depth of the coating spallation at these positions on the cooling efficiency of the blade is further considered.

Define r as the percentage of the localized spallation area of the coating to the surface area of the blade, which is shown as

$$r=\frac{S_1}{S}\times 100\% \tag{8}$$

where S represents the surface area of the blade, and S_1 the localized spallation area of the coating.

To investigate the influence of local coating spallation shape at different positions on the average surface temperature of the blade as the coating spallation thickness increases, three sets of rectangular and circular spallation shapes at different positions, as shown in Fig.7, are simulated under the condition of r=12%. It can be seen from Fig.9 that when the localized spallation position of the coating is located on the side close to the air conditioning inlet, that is, at positions 1′—5′ in Fig.8, the average temperature of the blade surface is the highest, followed by positions 1—5, and the lowest at positions 1″—5″. This indicates that the closer the coating spallation position is to the cooling air inlet side, the greater the impact on the cooling efficiency of the blade. When the coating is partially peeled off and approaches the air inlet of the cold air, it will cause the cold air to come into contact with the high-temperature blades without coating protection, raising the temperature of the cold air, reducing its convective heat transfer capacity, and thereby lowering the overall cooling efficiency of the cold air on blades.

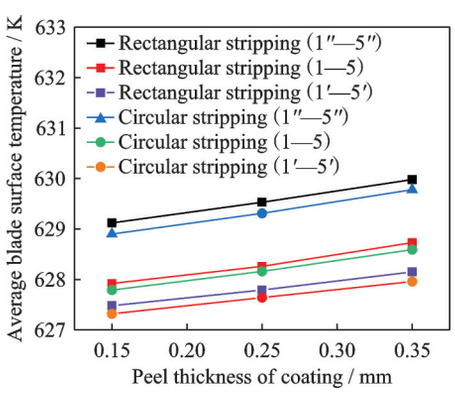

Fig.9 Influence of peel thickness and peel shape of the coating on the average surface temperature of the blade

When the localized spallation position of the coating is close to the air conditioning outlet, since the air conditioning has absorbed a large amount of heat from the blade at this time, the cooling efficiency deteriorates. Therefore, the impact of coating spallation at this point on the average temperature of the blade surface is relatively small.

For a fixed spallation site, the average blade surface temperature increases linearly with the progressive spallation thickness. When the proportion of the spallation area is constant and the spallation position is fixed, the shape of the spalled coating has a relatively small effect on the average surface temperature of the blade. The temperature difference between the average surface temperature of the blade with a rectangular and circular spallation shape is 0.1 K to 0.3 K. Thus, it can be seen that when the proportion of the localized spallation area of the coating is 12%, the contour of the localized spallation has a relatively small influence on the average temperature change of the blade surface. Therefore, further analysis is carried out subsequently based on the circular coating spallation as an example.

To explore the influence of the proportion r of the spallation area of different coatings on the average temperature of the blade surface with the change of spallation position, under the condition of a local coating spallation thickness of 0.35 mm, the localized spallation conditions of the coating under r of 3%, 6%, 9%, and 12% are simulated respectively. The results are shown in Fig.10. When the spallation position is fixed, the larger r is, the higher the average temperature of the blade surface is. The localized spallation of the coating at different positions has a greater impact on the average temperature of the blade surface. Moreover, the closer the spallation is to the cooling air inlet side, the greater the temperature increase caused by the localized spallation as the spallation area expands. This indicates that the average blade surface temperature is more significantly affected by the localized spallation area when it is closer to the cooling air inlet.

In order to explore the influence of different

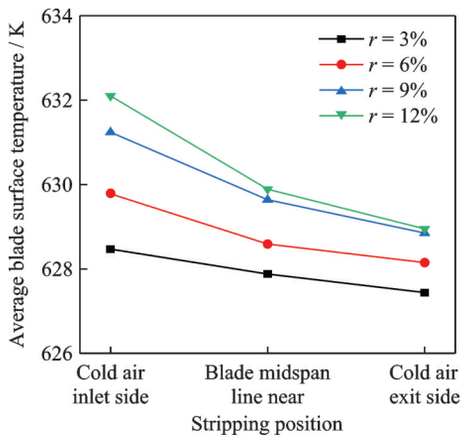

Fig.10 Influence of the peel position and peel area of the coating on the average surface temperature of the blade

spallation thicknesses and spallation areas of local coatings on the average temperature of the blade surface, three different thicknesses of simulated coatings of 0.15, 0.25, and 0.35 mm are selected for spallation on the side close to the air conditioning inlet, as shown in Fig.11. It can be seen from the figure that under a certain proportion of the local coating spallation area, the average temperature of the blade surface gradually increases with the increase of the spallation thickness, and the larger the r, the greater the temperature increase.

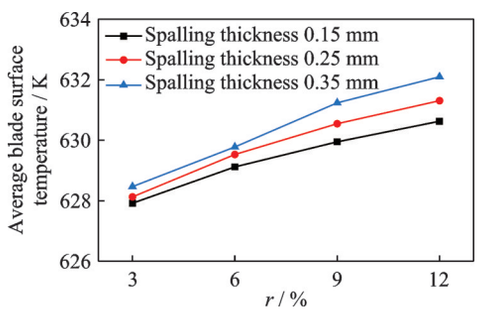

Fig.11 Influence of peel area and peel thickness of coating on average blade surface temperature

3 Rapid Prediction of Influence of Thermal Barrier Coating Spallation on Comprehensive Cooling Efficiency of Blades

3.1 Latin hypercube sampling method

Similar to biological networks, neural network learning is based on input and output[19]. Therefore, a dataset needs to be obtained before training a neural network, and a proxy model is constructed by conducting training, validation, and testing on the dataset. The verified proxy model can generate synthetic data, enhance the scale and diversity of the data set, and thereby improve the performance of the model[20]. Before constructing the proxy model, it is essential to sample the design space. Since the optimization problem typically involves multiple design variables, a multi-dimensional sampling method is commonly used. This work assumes that each design variable follows a uniform distribution within the design space, thereby introducing a special hierarchical Monte Carlo sampling method, namely Latin hypercube sampling (LHS). The LHS achieves uniform coverage of the entire parameter space by dividing the parameter space into multiple intervals of equal probability and ensuring that only one sample point is selected in each interval, thereby avoiding problems such as sample aggregation or omission of certain areas that may be caused by simple random sampling[21-22]. The LHS can be said to be one of the most effective small sample sampling methods[23].

In this work, the LHS method is used to perform stochastic sampling of the location, length, and depth of the localized coating spallation. The location of the localized spallation of the coating is determined by the distance between the centroid of the localized spallation and the leading edge stagnation point, denoted as L_p. The length of the localized spallation of the coating is determined by extending the same length in both directions along the leaf circumference from the centroid of the localized spallation, denoted as L_d. The spallation depth d is achieved by changing the surface thermal resistance, as shown in Fig.12. The value ranges of L_p and L_d are both $0—C_0$ (leaf circumference), and the value range of d is $0—d_{TBC}$ (total coating thickness). In order to facilitate the sampling, L_p, L_d, and d are are normalized into dimensionless quantities $\bar{L}_p$, $\bar{L}_d$, and $\bar{d}$ using Eqs.(9—11), respectively, constraining their value ranges to [0, 1].

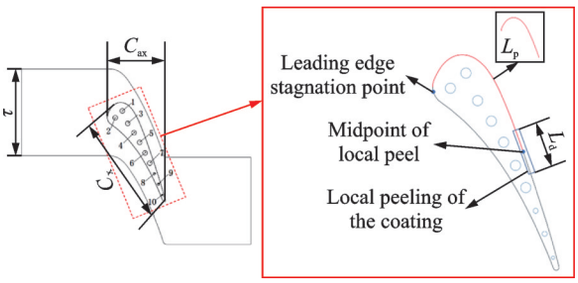

Fig.12 C3X blade model and localized spallation diagram of thermal barrier coating

$$\bar{L}_p = \frac{L_p}{c_0} \tag{9}$$

$$\bar{L}_d = \frac{L_d}{c_0} \tag{10}$$

$$\bar{d} = \frac{d}{d_{TBC}} \tag{11}$$

3.2 Prediction principle of MLP neural network

The multi-layer perceptron (MLP) neural network model utilizes a fully connected network structure, allowing it to effectively capture the feature relationships between multiple variables and the output. It is commonly used for logistic regression and nonlinear classification problems. Due to its simple network structure, ability to process data in paralle, and highly nonlinear global effects, MLP demonstrates strong classification performance. Fig.13 shows the prediction principle diagram of the MLP neural network in this work, which is composed of the input layer, the hidden layer and the output layer. Within the hidden layer, there are multiple layers with the same number of neurons. Neurons in the same layer are independent of each other, and neurons in each layer are fully connected to the neurons in the next layer. In the hidden layer, the neurons in the hidden layer perform weighted summation of the output values of each neuron in the previous layer, and then combine the activation function to perform nonlinear processing on the results, which are used as the input values of the subsequent layer. Among them, the input is $\{x_1, x_2, \cdots, x_n\}$, the weight of the jth neuron is $(w_{1j}, w_{2j}, \cdots, w_{nj})^T$, and the bias is b_i. The calculation process of each neuron from input to output is shown as

$$a_j = \sum_{i=j}^{n} w_{ji} x_i + b_j \tag{12}$$

$$y_j = f(a_j) \tag{13}$$

where a_j is the value obtained by weighted sum of the inputs of the neural tube numbered j and adding the bias b_j. After the activation by the activation function, the output y_j is obtained.

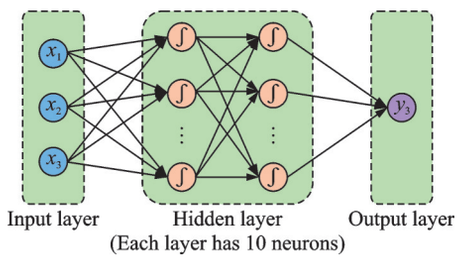

Fig.13 MLP neural network prediction model

Through the feature extraction and mapping between layers, the input values are propagated forward layer by layer. At the output layer, they are compared with the target values. The learning parameters in the neurons are updated in reverse according to the error gradient until the error meets the accuracy requirements. In the MLP neural network model of this work, the ReLU activation function, Adam optimization algorithm and MSE function are all adopted.

3.3 Establishment and verification of rapid prediction model

The LHS method is adopted to randomly sample the position, depth and length of localized spallation of the coating on the blade surface. The samples are calculated and the data are extracted through Fluent to generate a random data set for model training and parameter tuning. Then, based on the MLP neural network, an intelligent prediction model for the localized spallation temperature and cold effect distribution of the coating is constructed for the blade surface temperature and cold effect dataset after the localized spallation, to achieve rapid prediction of the influence of any coating spallation situation on cold effect.

In this work, the learning and prediction of seven parameters under 100 different spallation conditions are achieved through this model. 70% of the dataset is used as the training set, 20% as the validation set, and 10% as the test set. The training set

is primarily used to train the machine learning model, enabling it to learn and fit the mapping relationship between the input and output. The validation set is used to adjust the hyperparameters of the machine learning model and conduct a preliminary assessment of the model's ability to prevent the overfitting. The test set is only used to evaluate the generalization performance of the machine learning model. The specific definitions of the seven parameters are shown in Fig.14 and Table 4. In the figure, the blade surface is coated with a 0.35 mm thick coating based on the thin-wall thermal resistance model, where the red area represents the localized spallation area of the coating.

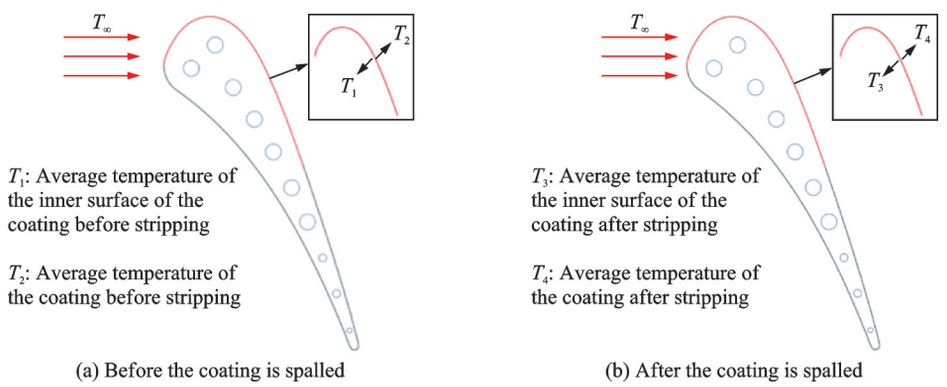

(a) Before the coating is spalled (b) After the coating is spalled

Fig.14 Schematic diagrams of parameter definitions before and after coating spallion

Table 4 Definiton of parameter names and meanings before and after coating spalltion

Parameter name	Definition
ϕ: Average cooling efficiency of blade surface	$\phi=\dfrac{T_\infty-T}{T_\infty-300}$
T_b: Average thermal insulation temperature of the coating before spallation	$T_b=T_2-T_1$
ϕ_b: Average cooling efficiency at the local peel of the coating before spallation	$\phi_b=\dfrac{T_\infty-T_b}{T_\infty-300}$
T_a: Average thermal insulation temperature of the the coating after spallation	$T_a=T_4-T_3$
ϕ_a: Average cooling efficiency at the local peel of the coating after spallation	$\phi_a=\dfrac{T_\infty-T_a}{T_\infty-300}$
ΔT_{max}: Maximum heat insulation temperature at localized spallation	$\Delta T_{max}=(T_4-T_3)_{max}$

The prediction error (ε) of this model is defined as the absolute value of the relative error between the predicted value (Z_{pre}) and the calculated value (Z_{cal}), as shown in Eq.(14). For the convenience of analysis, this work statistically analyzes the sample size (M_ε) within different error ranges and compares it with the total sample size (M_{total}).

$$\varepsilon=\left|\frac{Z_{pre}-Z_{cal}}{Z_{cal}}\times 100\%\right| \tag{14}$$

For this model, the following parameters are considered: The average surface temperature T of the blade, the average cold effect of the blade ϕ, the average heat insulation temperature T_b before spallation at the localized spallation site, the average heat insulation temperature T_a after spallation at the localized spallation site, the average cold effect before spallation at the localized spallation site ϕ_b, and the average cold effect after spallation at the localized spallation site ϕ_a. The relative error distribution of the training, verification and test results of the maximum temperature difference before and after spallation at the localized spallation area ΔT_{max} is shown in Fig.15. It can be seen from the figure that the prediction errors of the proxy model for T and ϕ of all datasets are both within 2%. In the training set, the maximum prediction error for T_b is within 10%, with an average error of 1.8%. The average prediction errors for T_a, ϕ_b, ϕ_a, and ΔT_{max} are 5.1%, 2.4%, 3.2%, and 5.5%, respectively, and

the errors of a few samples exceed 10%. In the validation set, the average prediction errors for T_b, T_a, ϕ_b, ϕ_a, and ΔT_{max} are 3.2%, 9.9%, 3.8%, 4.5%, and 9.2%, respectively. In the test set, the maximum prediction errors of ϕ_b, ϕ_a, and ΔT_{max} are all within 10%, with average prediction errors of 1.9%, 2.1%, and 3.2%, respectively. The average prediction errors of T_b and T_a are 2.8% and 5.4%, respectively, and the errors of a few samples exceed 10%. For the full random spallation of thermal barrier coatings, the prediction errors of ϕ_b and ϕ_a have the characteristics of relatively large errors and relatively small absolute errors. However, since the values of ϕ_b and ϕ_a are small and the variation range with different working conditions is relatively small, even a small absolute error can lead to a significant relative error. Therefore, this work considers that its prediction is still valid.

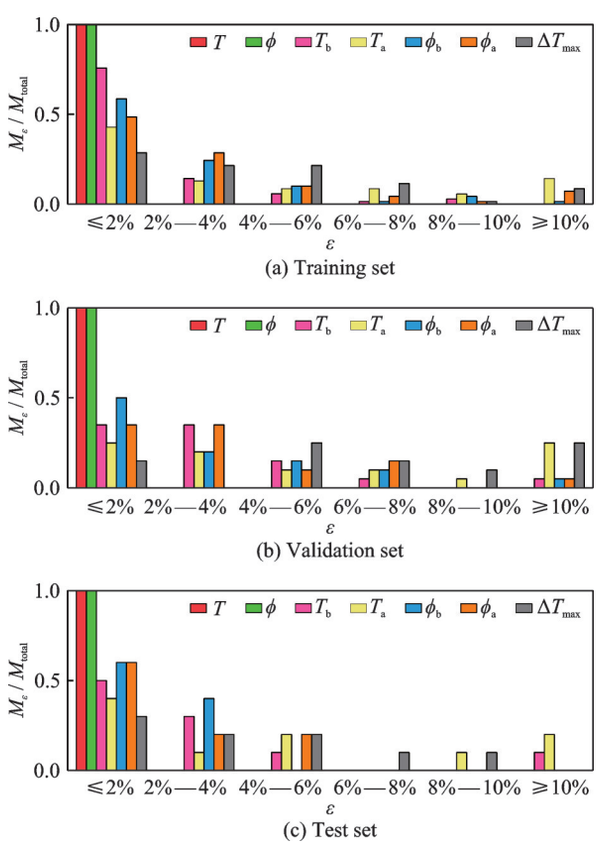

Fig.15 Proxy model prediction error distribution

Overall, the prediction error of this model for T and ϕ is within 2%, the prediction error for 80% of the samples of T_b, T_a, ϕ_b, and ϕ_a is within 6%, the average prediction error for all samples is within 10%, and the error for a few samples is above 10%. This model has a good prediction effect on T, ϕ, T_b, ϕ_b, and ϕ_a. However, at the localized spallation areas of the coating, the coating becomes thinner or completely peeled off, and the heat insulation capacity decreases. In contrast, there is a sudden increase in temperature at the coated areas, and the temperature change on the blade surface is uneven. The predictive ability of this model at the data step points is slightly poor, so the prediction error of T_a and ΔT_{max} is relatively large.

Figs.16 and 17 respectively show the relative error distributions of the average cold effect difference $\Delta\phi$ and the maximum cold effect difference $\Delta\phi_{max}$ before and after coating spallation in the localized spallation area trained with the MLP neural network. It can be seen from the figure that the relative errors of $\Delta\phi$ and $\Delta\phi_{max}$ are basically within 10%, and the errors of a few results exceed 10%. Compared with the parameters in Fig.16, the errors are slightly larger. For the random spallation of the thermal barrier coating, the prediction results of $\Delta\phi$ and $\Delta\phi_{max}$ show the characteristics of relatively large error and relatively small absolute error. However, since the values of $\Delta\phi$ and $\Delta\phi_{max}$ are relatively small and the changes are relatively small under different spallation conditions, even a small absolute error can lead to a large relative error. Therefore, we believe that the predictions of this study remain valid.

It can be seen from this that the prediction model of the localized spallation temperature and cold effect distribution of the coating based on the real

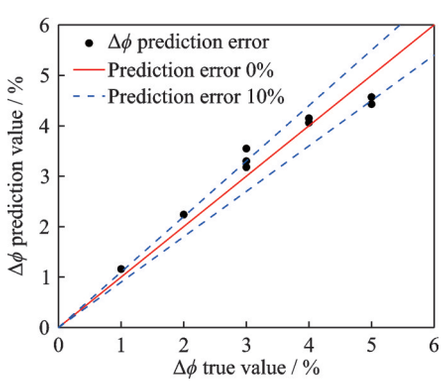

Fig.16 $\Delta\phi$ test set error distribution

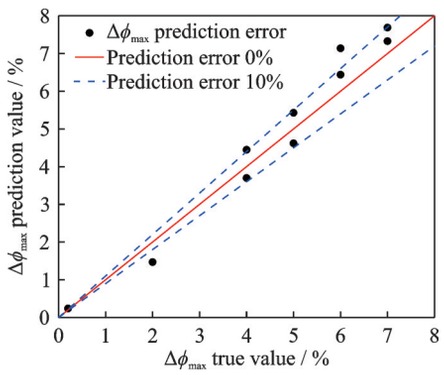

Fig.17 $\Delta\phi_{max}$ test set error distribution

state value has a high prediction accuracy, which will further support the establishment of the subsequent three-dimensional prediction model. Using this prediction model as the surrogate model in the case of arbitrary spallation of the coating can replace the mathematical model for efficient and high-precision regulation.

Simulation of thermal barrier coating failure on turbine blades shows that the coating at the leading edge of the blade is the most prone to peeling. However, after the coating in this tiny area peels off, since almost the entire blade surface is still protected and insulated by the coating, the turbine blade can continue to serve. As the service time increases, the area of coating spallation will continue to expand, leading to a higher probability of the blade being damaged by high temperatures. Once the spalled area reaches a critical threshold, the coating fails, and the blade is damaged. At present, some scholars have defined the spallation of the coating on 10% of the blade surface as failure, but this definition lacks the universality. Because the heat insulation effect of thermal barrier coating varies across different regions of the blade surface, spallation with the same area and depth can lead to markedly different reductions in blade cooling efficiency depending on its location; specifically, spallation occurring in a high-insulation-efficiency region causes a much larger decrease in cooling efficiency than spallation occurring in a low-insulation-efficiency region. Therefore, the proposed model enables rapid prediction of blade cooling efficiency under different spallation conditions, thereby better capturing the combined effects of spallation area, depth, and location on coating failure. This provides a more rational basis for failure assessment and is more consistent with practical service conditions. Subsequently, the mapping data relationship between the localized spallation characteristic parameters of the coating and the coating failure can be established. Data supports the coating reliability analysis and prediction.

3.4 Prediction results based on the fast prediction model

Due to the numerous factors influencing the spallation of coatings and the randomness of environmental parameters, there is uncertainty in the failure and spallation of coatings. However, the effects of coating failure and spallation at different positions on the surface of turbine blades on the comprehensive cooling efficiency of turbine blades are all different. In the previous section, the predictive ability of the proxy model is verified by comparing the error distributions of the true values and the predicted values. In this section, 1 000 groups of different coating spallation positions, coating spallation lengths and coating spallation depths are extracted by the LHS method. Based on the rapid prediction model of the influence of the trained thermal barrier coating spallation on the comprehensive cold efficiency of the blade, the influence of 0.35 mm local coating spallation on the comprehensive cold efficiency at the local coating spallation site of turbine blades is explored.

Fig.18 presents the influence of the spallation position and spallation length on the comprehensive cold effect difference at the spallation site under different coating spallation depths. Among them, c represents the percentage of the length along the leaf circumference starting from the retention point of the leading edge of the blade to the total leaf circumference length and its expression is given in Eq.(15). l represents the percentage of the spallation length to the total leaf circumference length and its expression is given in Eq.(16). $\Delta\phi$ is the difference in cold effect before and after the localized spallation of the coating.

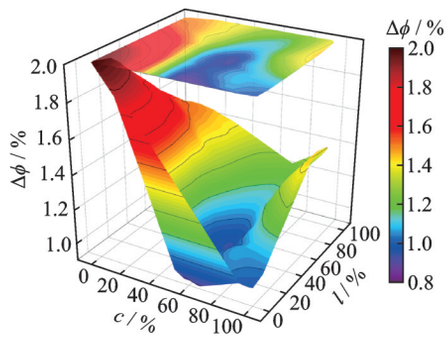

(a) The spallation depth is 30% of the coating thickness

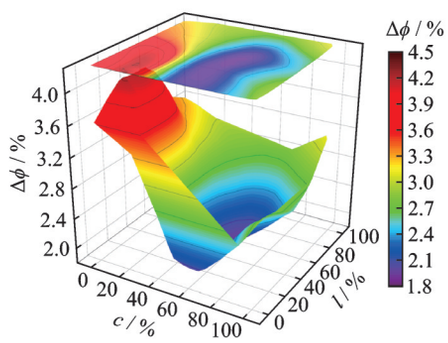

(b) The spallation depth is 60% of the coating thickness

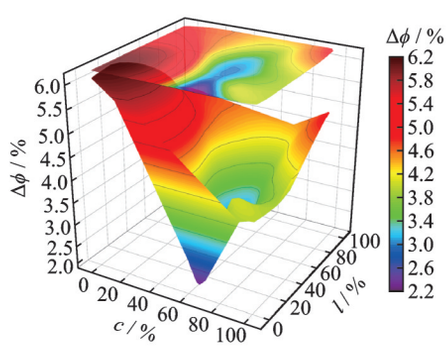

(c) The spallation depth is 90% of the coating thickness

Fig.18 Effect of spallation position and length on the overall cooling efficiency difference at different spallation depths

$$c = \frac{L_p}{c_0} \tag{15}$$

$$l = \frac{L_d}{c_0} \tag{16}$$

It can be seen from Fig.18 that with the increase of spallation depth, under different spallation positions and spallation lengths, the difference in cold effect before and after coating spallation at the localized spallation area of the coating gradually increases from 0.9% to 6.2%. Under the same spallation position and spallation length, for every 30% increase in the spallation depth of the coating, the difference in cooling efficiency before and after coating spallation increases by 1—2 times compared with the original cooling efficiency difference. When the spallation depth and spallation length of the coating are constant, the smaller the c value, that is, the closer the localized spallation position of the coating is to the leading edge, the greater the cold effect difference value, indicating that the coating at the leading edge position of the blade is crucial for the protection of the blade. When the c value is 60%—80%, the difference in cooling efficiency is the smallest, indicating that the spallation of the coating at the trailing edge of the blade and the middle and rear sections of the pressure surface has a relatively small impact on the cooling efficiency of the blade. When the coating spallation depth and spallation position are constant, the longer the coating spallation length at the leading edge, the less obvious the change in cold effect. The longer the coating spallation length at the trailing edge of the blade and the middle and rear sections of the pressure surface, the greater the change in cold effect. When the coating spallation depth accounts for 30% of the coating thickness, the average value of the difference in cooling efficiency before and after coating spallation is 1.32. When the spallation depth of the coating accounts for 60% of the coating thickness, the average value is 2.82. When the spallation depth of the coating accounts for 90% of the coating thickness, the average value is 4.48. For every 30% increase in the coating spallation depth, the average value of the difference in cooling efficiency before and after coating spallation doubles compared to the original value, that is, the influence degree of coating spallation on cooling efficiency doubles.

In conclusion, the coating spallation at the leading edge of the turbine blade has the greatest impact on the comprehensive cooling efficiency of the blade, while the coating spallation at the trailing edge has the least impact. The above research results have certain guiding significance for the subsequent differentiated coating in different zones, thereby reducing the impact of coating spallation on the cooling efficiency of the blade.

4 Conclusions

In this work, a rapid prediction model for the influence of localized spallation of thermal barrier coatings on the comprehensive cold efficiency of blades is constructed by combining the LHS method and the MLP neural network. The accuracy of the model is verified, and then the influence law of spallation in the dangerous area of thermal barrier coatings on the comprehensive cold efficiency of blades is obtained.

The following conclusions are obtained.

(1) It has been verified that the deviation of the thin-wall thermal resistance method and the direct modeling method of the coating is within 5% in the absence of coating spallation, and the deviation proportion is 6.2% in the case of localized spallation of the same coating. Therefore, the thin-wall thermal resistance model can be considered an effective simplification and replacement for the direct modeling method of the coating. When the localized spallation area of the coating is fixed, its shape has a relatively small influence on the blade's cooling efficiency. However, when the spallation position is fixed, the average blade surface temperature increases linearly with the spallation thickness.

(2) This work develops a rapid prediction model for the influence of localized spallation of thermal barrier coatings on blade temperature and cooling efficiency. The prediction error of this model for the average surface temperature of the blade and the cooling efficiency is within 2%. The estimation of the temperature and cooling efficiency at the localized spallation area of the coating shows that the error of 80% of the samples is within 6%, and the average error of all samples is within 10%.

(3) With the increase of the coating spallation depth, under different spallation positions and spallation lengths, the difference in cold effect before and after coating spallation at the localized spallation area of the coating gradually increases from 0.9% to 6.2%. The closer the localized spallation position of the coating is to the leading edge, the greater the difference in cooling efficiency. With each 30% increase in coating spallation depth, the average difference in cooling efficiency before and after spallation doubles compared to the original value, indicating that the impact of coating spallation on cooling efficiency also doubles.

References

[1] MEHTA A, VASUDEV H, SINGH S, et al. Processing and advancements in the development of thermal barrier coatings: A review[J]. Coatings, 2022, 12(9): 1318.

[2] WEI Z Y, MENG G H, CHEN L, et al. Progress in ceramic materials and structure design toward advanced thermal barrier coatings[J]. Journal of Advanced Ceramics, 2022, 11(7): 985-1068.

[3] LIU Jing, WANG Li, YU Minghan, et al. Research progress on the service environmental performance of nickel-based single crystal superalloys[J]. Materials China, 2024, 43(10): 891-901. (in Chinese)

[4] XU Guangnan. Chemo-thermo-mechanically coupling failure mechanism of thermal barrier coatings corroded by CMAS[D]. Xiangtan: Xiangtan University, 2021. (in Chinese)

[5] MAO W G, ZHOU Y C, YANG L, et al. Modeling of residual stresses variation with thermal cycling in thermal barrier coatings[J]. Mechanics of Materials, 2006, 38(12): 1118-1127.

[6] ZHOU Y C, HASHIDA T. Coupled effects of temperature gradient and oxidation on thermal stress in thermal barrier coating system[J]. International Journal of Solids and Structures, 2001, 38(24): 4235-4264.

[7] ASGHARI S, SALIMI M. Finite element simulation of thermal barrier coating performance under thermal cycling[J]. Surface and Coatings Technology, 2010, 205(7): 2042-2050.

[8] TANG W Z, YANG L, ZHU W, et al. Numerical simulation of temperature distribution and thermal-stress field in a turbine blade with multilayer-structure TBCs by a fluid-solid coupling method[J]. Journal of Materials Science & Technology, 2016, 32(5): 452-458.

[9] WEI Z Y, CAI H N, FENG R X, et al. Dynamic crack growth mechanism and lifetime assessment in plasma sprayed thermal barrier system upon temperature cycling[J]. Ceramics International, 2019, 45(12): 14896-14907.

[10] CHEN P, YUAN B, GUO X, et al. Interfacial spallation loads in the TBC with an air hole: Analytical so-

lutions and viscoplasticity modelling[J]. Ceramics International, 2022, 48(19): 27388-27400.

[11] ARAI M. Microdamage-coupled inelastic deformation analysis of ceramic thermal barrier coatings subjected to tensile loading[J]. Surface and Coatings Technology, 2016, 304: 542-552.

[12] LIU Y, CHEN K, KUMAR A, et al. Principles of machine learning and its application to thermal barrier coatings[J]. Coatings, 2023, 13(7): 1140.

[13] YANG L, KANG H S, ZHOU Y C, et al. Intelligent discrimination of failure modes in thermal barrier coatings: Wavelet transform and neural network analysis of acoustic emission signals[J]. Experimental Mechanics, 2015, 55(2): 321-330.

[14] LIU Z Y, YANG L, ZHOU Y C. A multiscale model integrating artificial neural networks for failure prediction in turbine blade coatings[J]. Surface and Coatings Technology, 2023, 457: 129218.

[15] RANJBAR-FAR M, ABSI J, MARIAUX G, et al. Effect of residual stresses and prediction of possible failure mechanisms on thermal barrier coating system by finite element method[J]. Journal of Thermal Spray Technology, 2010, 19(5): 1054-1061.

[16] HYLTON L D, MIHELC M S, TURNER E R, et al. Analytical and experimental evaluation of the heat transfer distribution over the surfaces of turbine vanes: NASA-CR-168015[R]. Cleveland, USA: NASA Lewis Research Centre, 1983.

[17] WANG Y Q, WANG F L, WANG Y B, et al. Numerical study on the effect of partial delamination of thermal barrier coating on the cooling effect of turbine blade[J]. Journal of Physics: Conference Series, 2023, 2610: 012029.

[18] CROSBY J M. Particle size, gas temperature, and impingement cooling effects on highpressure turbine deposition in land based gas tubines from various synfuels[D]. Provo: Brigham Young University, 2007.

[19] WAQAR T, DEMETGUL M. Thermal analysis MLP neural network based fault diagnosis on worm gears[J]. Measurement, 2016, 86: 56-66.

[20] FURTNEY J K, THIELSEN C, FU W, et al. Surrogate models in rock and soil mechanics: Integrating numerical modeling and machine learning[J]. Rock Mechanics and Rock Engineering, 2022, 55(5): 2845-2859.

[21] WU C, ZHU M, TAN Q, et al. A comprehensive study of non-adaptive and residual-based adaptive sampling for physics-informed neural networks[J]. Computer Methods in Applied Mechanics and Engineering, 2023, 403: 115671.

[22] MCKAY M, BECKMAN R, CONOVER W. A comparison of three methods for selecting vales of input variables in the analysis of output from a computer code[J]. Technometrics, 1979, 21: 239-245.

[23] HELTON J C, DAVIS F J. Latin hypercube sampling and the propagation of uncertainty in analyses of complex systems[J]. Reliability Engineering and Safety System, 2003, 81(1): 23-69.

Acknowledgements This work was supported by the National Natural Science Foundation of China (No.52206090), the Jiangsu Provincial Natural Science Foundation (No. BK20220901), the National Major Science and Technology Projects of China (No.Y2022-Ⅲ-0004-0013), Engineering Research Center of Low-Carbon Aerospace Power Ministry of Education (No.CEPE2024020), and the China Postdoctoral Science Foundation (No.2022TQ0149).

Authors

The first author Ms. **ZHANG Yeling** received the B.S. degree in oil and gas storage and transportation engineering from Southwest Petroleum University in 2023 and now she is pursuing the M.S. degree in power engineering and engineering thermophysics at Nanjing University of Aeronautics and Astronautics (NUAA). Her research interest is focused on the simulation and experimental study on the influence of thermal barrier coating deposition failure based on gas-thermal-solid coupling on the overall cooling efficiency of blades.

The corresponding author Dr. **WANG Feilong** received the Ph.D. degree from Xi'an Jiaotong University in 2019. He joined in NUAA in March 2020, where he is an associate professor of College of Energy and Power. His research is focused on ash accumulation and heat transfer recession on heat transfer surfaces. In 2021, he was awarded the "Double Creation Doctor" talents in Jiangsu Province. In 2022, he was awarded the 8th China Association for Science and Technology (CAST) Young Talent Support Project for the Aerospace Development Industry-Academia Consortium.

Author contributions Ms. **ZHANG Yeling** completed the model construction and verification, analyzed the numerical calculations, explained the results, and wrote the manuscript. Mr. **WANG Yuqun**, Mr. **WANG Yubin** and Dr. **WANG Feilong** provided data for the construction of the thin-wall thermal resistance model. Dr. **WANG Feilong** and Prof. **MAO Junkui** evaluated the manuscript draft. All au-

thors commented on the manuscript draft and approved the submission.

Competing interests The authors declare no competing interests.

(Production Editor: WANG Jing)

基于MLP神经网络的热障涂层局部剥离对叶片冷效影响的快速预估

张烨苓[1], 王飞龙[1], 王于群[2], 王玉彬[1], 毛军逵[1]

(1.南京航空航天大学能源与动力学院,南京 210016,中国;
2.中国航发四川燃气涡轮研究院,成都 610500,中国)

摘要:涡轮叶片表面热障涂层的剥离及其影响的研究对于燃气轮机安全运行具有重要意义,然而热障涂层有关数值模拟难度大、时间成本高,难以满足工程需求。为此本文建立了基于薄壁热阻模型的叶片热障涂层局部剥离对表面温度及冷效的快速预测模型。首先,数值研究了典型涡轮叶片表面热障涂层局部剥离对冷效的影响;接着,基于仿真数据集及MLP神经网络,构建了涂层局部剥离温度及冷效分布智能预估模型,可实现对叶片表面任意位置涂层剥离情况下叶片表面温度及冷效的快速预估。研究结果表明,在一定的剥离面积下,涂层局部剥离形状对冷效影响小,而剥离厚度的增加会使叶片表面平均温度线性上升;所提出的快速预估模型对叶片表面平均温度及冷效预估误差在2%以内,而对于80%的样本,涂层局部剥离处温度及冷效预估误差在6%内,总体平均误差在10%以内;由快速预估模型得出,涂层剥离深度增加时,剥离位置越靠近叶片前缘,冷效差值越大,且涂层剥离对冷效影响程度随之增加。

关键词:热障涂层;冷却性能;快速预测;MLP神经网络